Journal of
Medicinal Chemistry

Article

Azo-PROTAC: novel light-controlled small-molecule tool for protein knockdown

Yuhui Jin, Mengchen Lu, Yan Wang, Wenxin Shan, Xuanyu Wang, Qi-Dong You, and Zhengyu Jiang

J. Med. Chem., **Just Accepted Manuscript** • DOI: 10.1021/acs.jmedchem.9b02058 • Publication Date (Web): 10 Mar 2020

Just Accepted

is published by the American Chemical Society. 1155 Sixteenth Street N.W., Washington, DC 20036

Azo-PROTAC: novel light-controlled small-molecule tool for protein knockdown

Yu-Hui Jin,[a,b,‡] Meng-Chen Lu,[a,b,‡] Yan Wang,[a,b] Wen-Xin Shan,[a,b] Xuan-Yu Wang,[b] Qi-Dong You,[a,b,] and Zheng-Yu Jiang,[a,b,*]*

[a] State Key Laboratory of Natural Medicines and Jiang Su Key Laboratory of Drug Design and Optimization, China Pharmaceutical University, Nanjing 210009, China.

[b] Department of Medicinal Chemistry, School of Pharmacy, China Pharmaceutical University, Nanjing 210009, China.

KEYWORDS: protein knockdown; photoswitchable PROTAC; protein modifications; ubiquitin-proteasome system.

ABSTRACT: Reversibly altering endogenous protein levels are persistent issues. Herein, we designed photoswitchable Azo-PROTACs by including azobenzene moieties between ligands for the E3 ligase and the protein of interest. Azo-PROTACs are light-controlled small-molecule tools for protein knockdown in cells. The light-induced configuration change can switch the active state to induce protein degradation activity, which can be reversely controlled by light exposure in intact cells. We compared the protein degradation abilities of Azo-PROTACs with different configurations and linker lengths. Using the stable form with the best degradation ability against the BCR-ABL fusion and ABL proteins in myelogenous leukemia K562 cells, we showed that

Azo-PROTAC combines the potent protein knockdown and facile cell uptake properties of the small-molecule PROTAC with a reversible photo-switch ability, offering a promising chemical knockdown strategy based on the light-induced reversible on/off property.

Introduction

Conditional knockdown tools are fundamental to reveal specific protein functions in complex biological systems.[1] Two main approaches are currently used to disrupt protein function[2]: DNA-modifying methods can knockout proteins at the genome level[3] and RNA interference can be used to knockdown protein expression by disrupting the mRNA level[4]. Recently, several protein-targeting technologies have been applied for inducing protein degradation. For example, Proteolysis Targeting Chimeras (PROTACs) can recruit the E3 ligase to a protein of interest, leading to its degradation via the ubiquitin-proteasome system.[5-8] Low-molecular-weight hydrophobic tags (HyTs) can promote labeled protein degradation since exposed hydrophobic regions are a hallmark of unfolded proteins, signaling their elimination by the ubiquitin-proteasome system or autophagy.[9] TRIM-Away is another protein-targeted knockdown strategy that can harness the cellular protein degradation machinery to remove unmodified native proteins within only minutes. However, these approaches cannot achieve the simultaneous potent downregulation activity, facile cell uptake, and reversible control for protein knockdown that are required in research applications.[2] Thus, how to find a reversible and controllable small-molecule protein depletion method that acts exclusively at the protein level currently needs to uncover. Such a method would not only allow for the depletion of proteins but also allow artificial termination of the degradation process if necessary.

Cellular activities are mediated by multiple biochemical pathways involving a network of biomolecules that communicate in a temporally and spatially well-defined fashion.[10] Conventional approaches to knocking out a specific biomolecule in cells and traditional inhibitor-based therapeutics may have undesired effects because systemic application can affect untargeted tissue.[11] Introducing a switchable element within molecular biology tool can allow reversible degradation in a spatiotemporal manner.[11] A typical design strategy has emerged based on the fusion of a sensory domain with an effector domain to create a chimera such as photo-caging[12] and photosensitive degrons[13-16]. Here, we sought to develop an adjustable protein depletion method based on controllable small-molecular devices. Diverse triggers[17-21] or switch modules[22-25] have been introduced in various biofunctional molecules to regulate different targets. Among these modules, using a photoswitch has the advantages of reversibility, speed, and facile modulation of the energies involved.[26] Over the past decade, various photoswitches with excellent pharmacodynamic and pharmacokinetic properties, such as azobenzene (Azo), have been applied to a wide range of biological targets. These studies include transmembrane proteins (G protein-coupled receptors[27-30], ion channels[31-34], transporters[35, 36], and receptor-linked enzymes[37]), soluble proteins (kinases[38-40], proteases[41-43], and factors involved in epigenetic regulation[44-46]), lipid membranes[47], and nucleic acids[48-50]. Therefore, we designed photoswitchable Azo-PROTACs by including azobenzene moieties between ligands for the E3 ligase and the protein of interest for targeted and reversible protein degradation.

The ABL and BCR-ABL proteins are expressed in many cases of chronic myelogenous leukemia (CML)[51, 52] and have thus emerged as pioneering targets for PROTAC-based research. In 2015, Crews group first designed DAS-CRBN and BOS-CRBN PROTACs to knockdown the BCR-ABL fusion protein and found that these PROTACs could effectively degrade BCR-ABL and ABL

proteins even at extremely low levels.[52] In 2016, Naito group developed PROTACs by conjugating Imatinib[53] and Dasatinib[54] to IAP ligands, which induced the reduction of BCR-ABL protein in K562 cells. In 2019, Jiang group designed PROTACs targeting BCR-ABL which connected Dasatinib and ligand of E3 ligase Von Hippel-Lindau (VHL).[55] Meanwhile, Crews group developed PROTACs that allosterically target BCR-ABL1 protein and recruit the VHL E3 ubiquitin ligase, resulting in degradation of the fusion protein.[56] ABL has also been implicated in the response to growth factors[57], cytokines[58], cell adhesion[59], DNA damage[60], oxidative stress[61], and other physiologically important signals. Therefore, excessive knockdown of ABL may also affect the normal physiological function of the body. Accordingly, the aim of the present study was to develop a controllable PROTAC targeting BCR-ABL as a conditional and reversible small-molecule protein knockdown tool, which can further be used to explore the therapeutic potential of BCR-ABL degraders.

RESULTS AND DISCUSSION

Design of Azo-PROTACs

Lenalidomide, a derivative of pomalidomide, is frequently used in PROTACs to interact with the ubiquitin E3 ligase cereblon.[62-64] Analysis of the X-ray crystal structure of cereblon in complex with Lenalidomide (**Figure 1A**, PDB ID: 4TZ4) revealed that the Lenalidomide-binding pocket was extremely small, and showed strong steric hindrance at the solvent boundary. Therefore, we attached the Azo unit at the 3-position of the phenyl in Lenalidomide. This strategy assumed that the configuration changes of the Azo unit might cause a great difference in degradation activity after conjugating protein-targeting ligands at the other side of the linker.

Dasatinib, targeting to ABL protein (**Figure 1B**), was the second-generation tyrosine kinase inhibitor developed to treat CML patients with acquired resistance to imatinib, and it has ever been used in DAS-CRBN PROTAC degrading BCR-ABL fusion protein. The docking results showed that after conjugating dasatinib at the other side of the linker, only the trans-configuration was combinative due to steric hindrance (**Figure 1C**). This implied that the trans and cis configurations of Lenalidomide-Azo might show great differences in degradation activity after conjugating dasatinib at the other side of the linker.

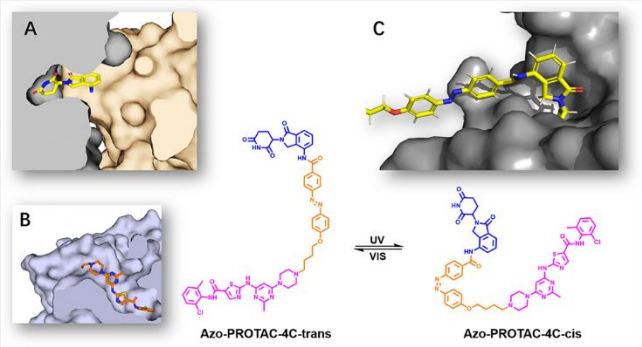

Figure 1. A) Crystal structure of Human Cereblon in complex with DDB1 and Lenalidomide (PDB ID: 4TZ4); B) Cocrystal structure of Dasatinib bound ABL protein (PDB ID:2GQG); C) Docking simulation of Azo-PROTAC-4C-trans and Cereblon.

Screening for a linker of suitable length via immunoblotting

To find the suitable length of the linker, we first synthesized Azo-PROTAC-2C (**Figure 2A**), the shortest of all dasatinib-Azo-lenalidomide trifunctional molecules, and tested its ability for ABL and BCR-ABL degradation in cell culture via immunoblotting. For this purpose, we chose the myelogenous leukemia cell line K562, which has been proven to express ABL and BCR-ABL together with the E3 ligase CRBN.[52, 54, 65] Indeed, Azo-PROTAC-2C induced a dramatic decrease

in the levels of both ABL protein and the BCR-ABL fusion protein at 100 nM after 36-hours treatment (**Figure SI 2A**). We then extended the linker between dasatinib and the Azo unit (**Scheme 1**), and found that Azo-PROTAC-4C exhibited the best activity in degrading the BCR-ABL fusion protein among the various PROTACs tested (**Figure 2B**).

Scheme 1. Synthetic Route of Azo-PROTAC

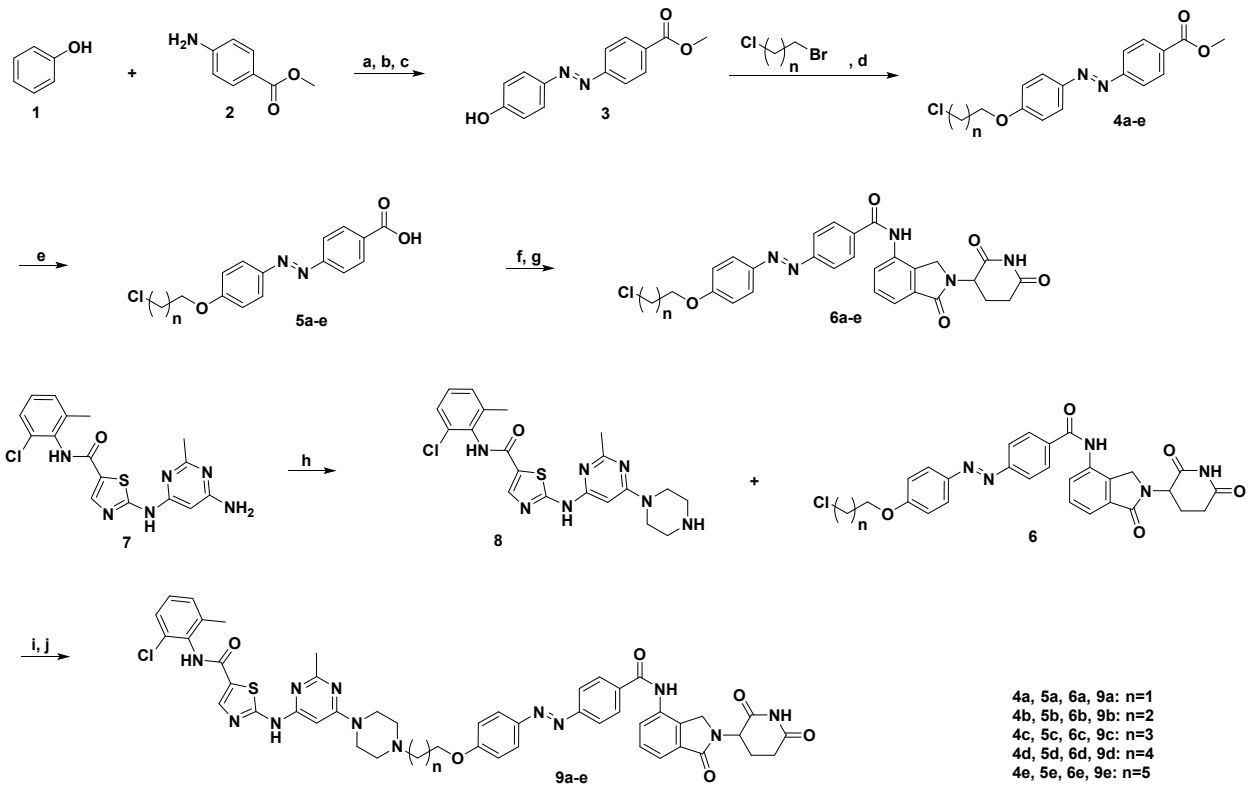

Reagents and conditions: a) HCl, $NaNO_2/H_2O$, 1h; b) Cs_2CO_3, H_2O, rt, 3h; c) AcOH, H_2O, pH=4; d) K_2CO_3, DMF; e) LiOH, THF : H_2O = 1 : 1, r.t., overnight; f) $(COCl)_2$, DMF(cat), DCM; g) Lenalidomide, DIEA, THF, rt., 8h; h) Piperazine, DIEA, Dioxane, reflux, 24h; i) NaI, Acetone, reflux, 24h; j) DIEA, DMF, 16h.

Photoisomerization kinetics

To explore whether Azo-PROTAC-4C can switch the configurations in a stable and controllable manner, we investigated its photoisomerization kinetics characteristic through analysis of UV-visible absorption spectra. The trans isomer of Azo-PROTAC-4C exhibited maximal absorption (λ_{max}) of the Azo unit at 361 nm. When exposed to UV-C light, the peak at 361 nm decreased by varying degrees over time, indicating formation of the cis isomer (**Figure 2E**). The plot of absorbance at 361 nm versus time indicated that 1-hour exposure was sufficient to convert 4C-

trans into 4C-cis (**Figure 2F**). We next exposed 4C to white light, which transformed into the cis-configuration within 4 hours (**Figure 2G**). In addition, as 4C is a T-type photo-switch, we further investigated its spontaneous thermal relaxation (from cis to trans) in dark conditions. The measured half-life of spontaneous thermal relaxation was approximately 620 min at 25°C, which was sufficiently long to conduct the subsequent experiments. (**Figure SI 1A**). Moreover, 4C was stable across five switching cycles (**Figure SI 1C**). We also tested the stability of 4C to reduction by glutathione (GSH). 4C was incubated in 20 mM of GSH reduced in a dimethyl sulfoxide (DMSO)/phosphate-buffered saline (PBS) buffer (1:1) solution, and no obvious difference was observed in 48 hours (**Figure SI 1B**), demonstrating its good stability.

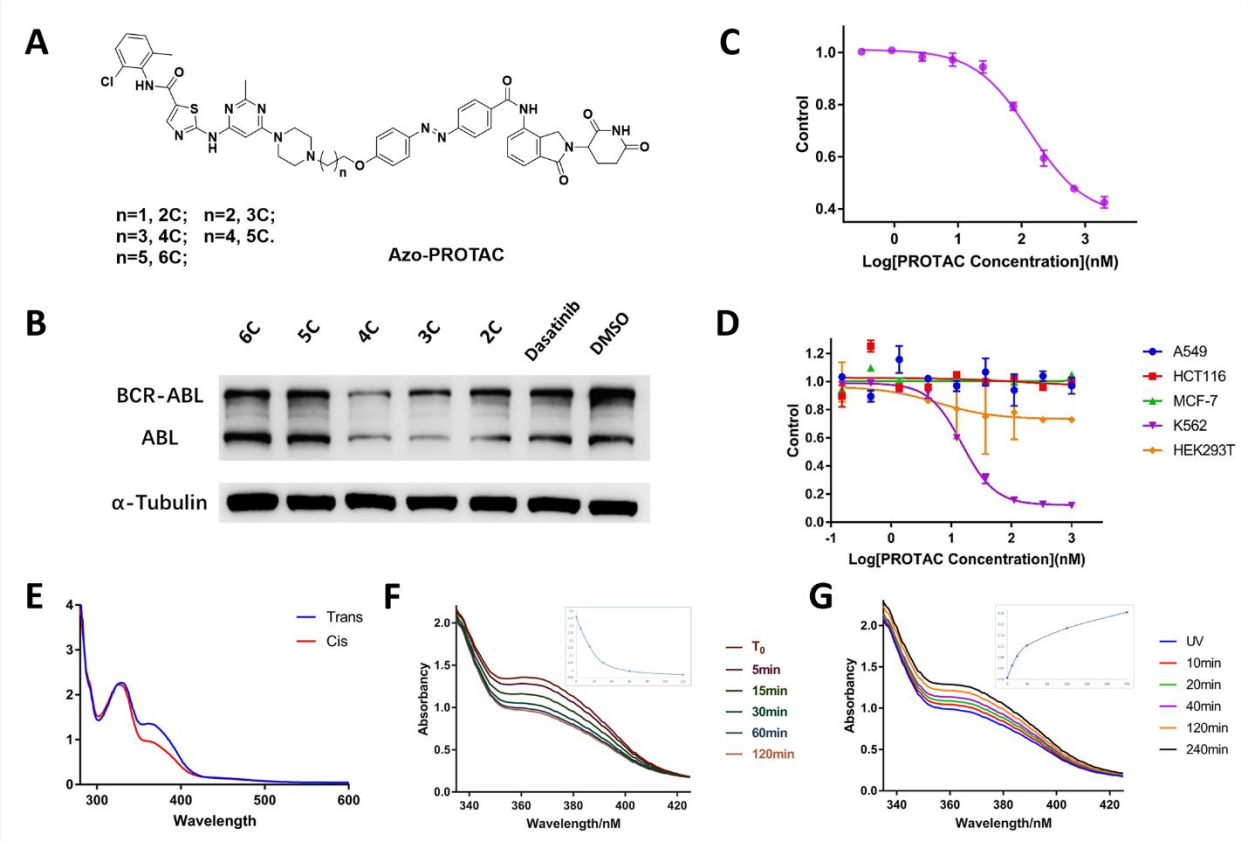

Figure 2. A) Structure of photoswitchable PROTACs; B) Western blot analysis of BCR-ABL and ABL after treating different compounds at 100 nM for 24 hours; C) Cell proliferation assay of Azo-PROTAC-4C-trans for K562 cell line; D) Cell viability assay of Azo-PROTAC-4C-trans for A549, HCT116, MCF-7, HEK293T and K562 cell lines; E) UV−visible absorption spectroscopy of 4C-trans and 4C-cis; F) UV−visible absorption spectroscopy of Azo-PROTAC-4C-trans exposed to UV-C light at different time; G) UV−visible absorption spectroscopy of Azo-PROTAC-4C-cis exposed to white light at different time points.

Azo-PROTAC-4C acts selectively on a BCR-ABL-driven K562 cell line

We next evaluated the cellular effects of the PROTAC. Azo-PROTAC-4C showed great potency against BCR-ABL-driven K562 cells with a half-maximal inhibitory concentration (IC_{50}) of 68 nM in a cell proliferation assay (**Figure 2C**) and a half-maximal response concentration (EC_{50}) of 28 nM in a cell viability assay (**Figure 2D**). Furthermore, 4C did not affect any of the non-BCR-ABL-driven cell lines tested, such as A549 pulmonary carcinoma cells, HCT116 colorectal carcinoma cells, and MCF-7 breast carcinoma cells (**Figure 2D**). Thus, this PROTAC retains selective activity against the BCR-ABL-driven cell line K562.

Azo-PROTAC-4C can induce CRBN ubiquitination and proteasome-mediated degradation of BCR-ABL and ABL

The mechanism of action of BCR-ABL protein degradation by Azo-PROTAC-4C was further investigated. Addition of the ABL inhibitor Dasatinib effectively blocked the degradation of BCR-

ABL and ABL proteins induced by Azo-PROTAC-4C (**Figure 3C**), confirming that the degradation of ABL proteins by Azo-PROTAC-4C requires its binding to ABL proteins. To establish the specificity of Azo-PROTAC-4C, we synthesized Azo-PROTAC-4C (-) (**Scheme 2**), with N-methylated modification of the glutarimide, as a negative control in this experiment. Compared to Azo-PROTAC-4C (+), no degradation of BCR-ABL and ABL proteins were observed at different concentrations of Azo-ROTAC-4C (**Figure 3A**). Similarly, addition of Lenalidomide also effectively hindered the degradation induced by Azo-PROTAC-4C for all proteins (**Figure 3D**), indicating that degradation of BCR-ABL proteins by Azo-PROTAC-4C is cereblon-dependent. The NEDD8-activating enzyme (NAE) inhibitor MLN4924 also completely blocked the degradation of BCR-ABL proteins by Azo-PROTAC-4C (**Figure 3B**), indicating that BCR-ABL and ABL protein degradation by Azo-PROTAC-4C depends upon NAE. These mechanistic data constitute clear evidence that Azo-PROTAC-4C is a bona fide CRBN-dependent ABL degrader.

Scheme 2. Synthetic Route of Azo-PROTAC-4C（-）

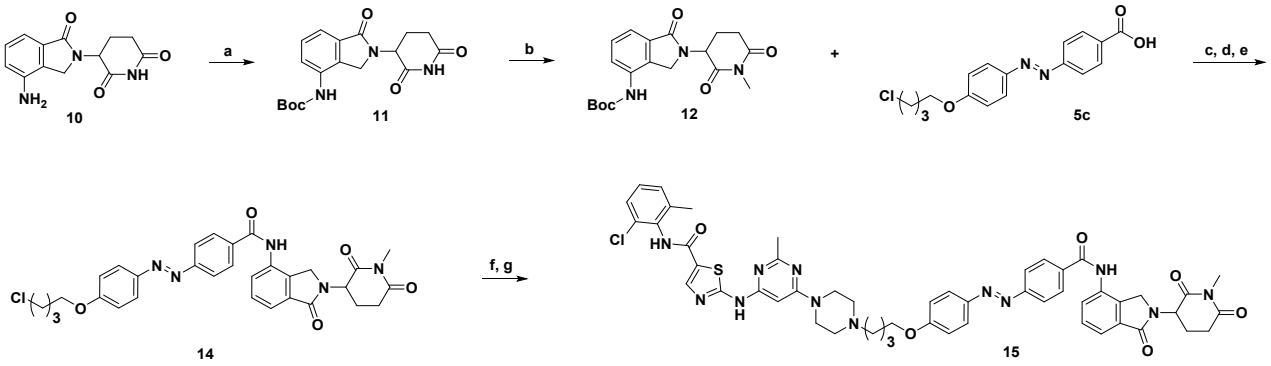

Reagents and conditions: a) $(Boc)_2O$, DMF, 6h; b) Cs_2CO_3, CH_3I, DMF, overnight; c) HCl/EA, DCM, 4h; d) $(COCl)_2$, DMF(cat), DCM; e) DIEA, THF, r.t. , 8h; f) NaI, Acetone, reflux, 24h; g) DIEA, DMF, 16h.

Trans- and cis-configurations of Azo-PROTAC-4C show great difference in degrading targeting proteins

Next, we tested the difference of ABL and BCR-ABL degradation activity between the 4C-cis and 4C-trans configurations. For 4C-trans, slight degradation of the BCR-ABL fusion protein was observed at a concentration of 25 nM, and remarkable reductions of BCR-ABL and ABL were observed at a 4C concentration of 100 nM in a dose-effect evaluation (**Figure 3G**). However, under the same condition, no notable degradation of BCR-ABL was observed with 4C-cis, even at the highest concentration of 500 nM (**Figure 3H**). Time-course analysis to assess the temporal degradation of ABL and BCR-ABL proteins showed that with 4C-trans, the ABL protein clearly decreased after 4-h treatment, both BCR-ABL and ABL proteins were significantly degraded after 10-h treatment, and more than 90% degradation of BCR-ABL was observed after 32-h treatment (**Figure 3E**). By contrast, no noticeable reduction of BCR-ABL was observed until 32 h of treatment with the 4C-cis group (**Figure 3F**). In addition, the results of RT-qPCR revealed that Azo-PROTAC-4C did not affect the expression of ABL gene (**Figure S4A & S4B in the SI**). Collectively, these results proved that the trans and cis configurations of 4C show substantially different degradation activities and that only the trans-configuration was effective.

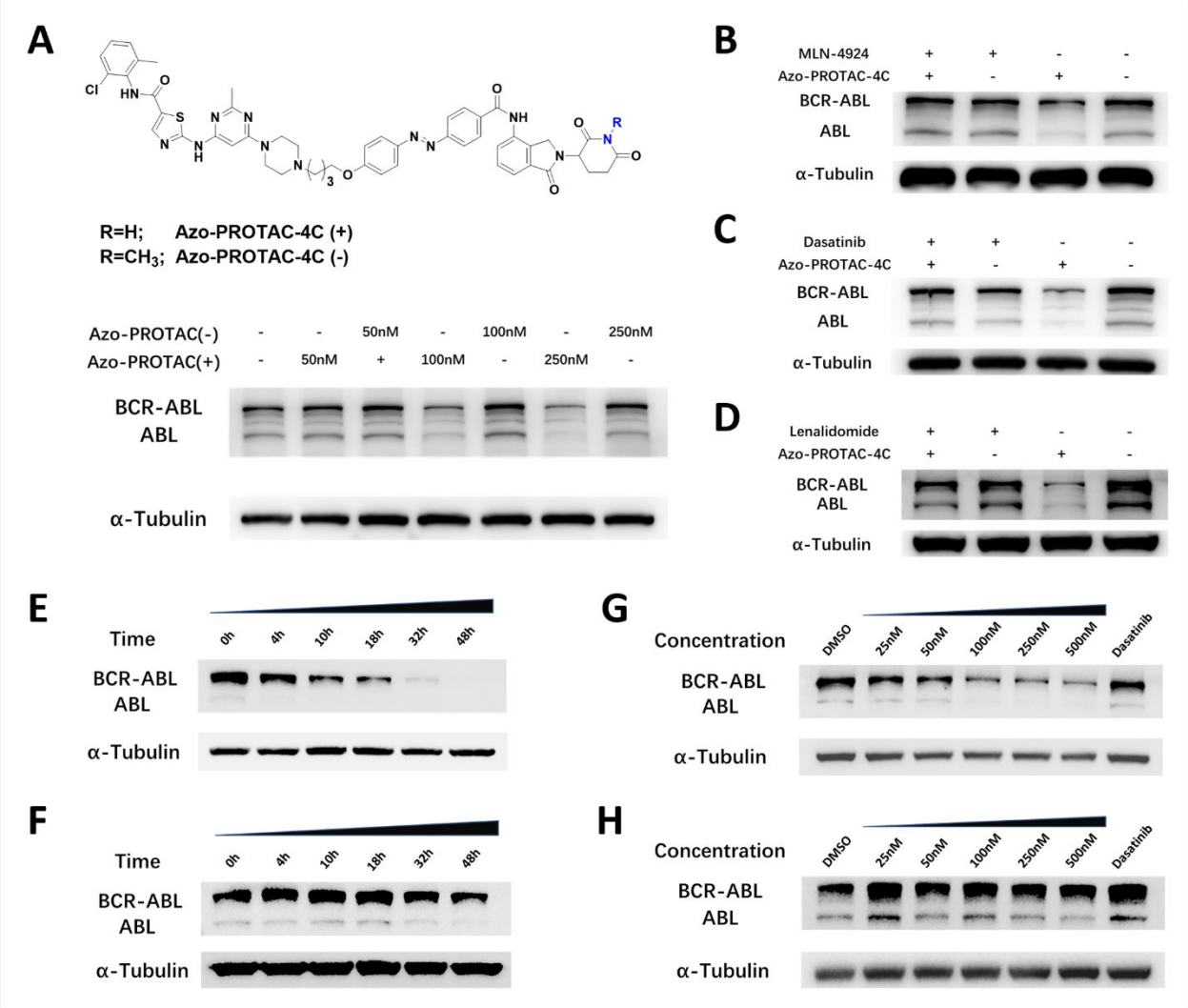

Figure 3. A) Western blotting analysis of BCR-ABL and ABL protein after treating Azo-PROTAC-4C (+)/(-); Western blotting analysis of BCR-ABL and ABL proteins after a 2-hour pretreatment with a NEDD8-activating enzyme (NAE) inhibitor MLN4924MLN-4924 (B), Dasatinib (C) or Lenalidomide (D), followed by a 24-hour treatment with Azo-PROTAC-4C at 250 nM in K562 cells; Time-course Western blot of Azo-PROTAC-4C-trans (E) or Azo-PROTAC-4C-cis (F) at 250 nM PROTAC concentration; Western blot of Azo-PROTAC-4C-trans (G) and Azo-PROTAC-4C-trans (H) for K562 cell line after 24h-treatment in concentration gradient.

Active state of Azo-PROTAC switched by UV irradiation in live cells

Finally, to evaluate the reversible character of the photoswitchable Azo-PROTAC-4C, we simulated the light control process. After treating K562 cells with 4C-trans for 24 hours, the cells were transferred to fresh medium and divided into two groups: one group that was harvested and exposed to UV-C light every 4 hours and the other group that was harvested for 0, 4, 8, 12, 16, and 24 hours as a control. In the UV-irradiated group, the levels of ABL and BCR-ABL increased over time (**Figure 4B UV-Group)**, whereas in the white light control group, the BCR-ABL fusion protein and ABL protein were maintained at low levels (**Figure 4B VIS-Group**). Similarly, we tried to trigger Azo-PROTAC-4C-cis in K562 cells. After preincubating 4C-cis shielded from light，the cells were transferred to fresh medium and exposed to visible light. Whereafter, BCR-ABL was degraded with time (**Figure 4A**). These results strongly supported that the UV light-induced configuration change of 4C could control its degradation activity, which can make the PROTAC-induced protein knockdown a reversible process.

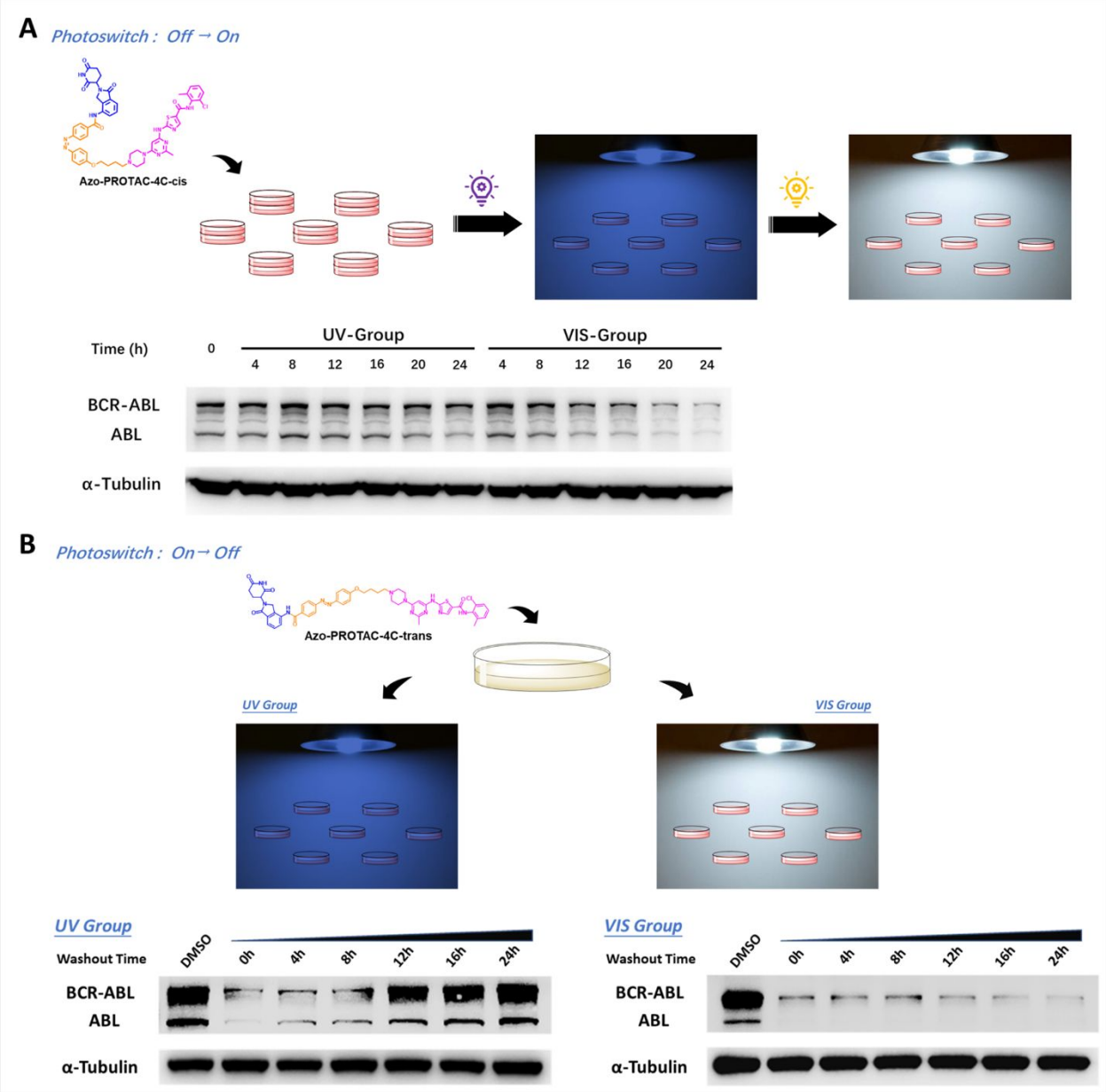

Figure 4. A) Western blotting alaysis of light-triggerring process in K562 cells; B) Western blotting alaysis of Azo-PROTAC-4C in white light (VIS-Group) and exposed to UV every 4 hours (UV-Group) for K562 cells after 24h-treatment.

Conclusion

We developed a novel small-molecule tool, Azo-PROTAC, to adjust the protein degradation process simply using UV light. Utilizing the lenalidomide-Azo-dasatinib trifunctional system, we demonstrated that the trans and cis isomers of Azo-PROTAC have marked differences in protein degradation activity, and we could control the degradation of ABL and BCR-ABL proteins by changing the configuration of Azo-PROTAC with UV-C light. On this basis, we further confirmed that the active state of Azo-PROTAC can be switched by UV irradiation in live cells.While in the process of preparing this manuscript, we became aware that Grews' s Group had reported bistable PhotoPROTACs.[11, 66] Besides, many scientific studies undertaken similar investigations and have achieved great processes.[67-69] As is shown in these studies, the combination of PROTACs and photopharmacology has led us to develop the concept of photoswitchable, stable degraders with potentially far reaching implications for manifold applications.[11]

EXPERIMENTAL SECTION

Chemistry. General Methods. All reactions were carried out under an atmosphere of dry nitrogen. Glassware was oven-dried prior to use. Unless otherwise indicated, common reagents or materials were obtained from commercial source and used without further purification. *N, N*-Diisopropylethylamine (DIPEA) was obtained anhydrous by distillation over potassium hydroxide. Tetrahydrofuran (THF), Dichloromethane (CH_2Cl_2), acetonitrile (CH_3CN) and dimethylforamide (DMF) was 99.5%, Extra Dry, with molecular sieves, Water$\leqslant$50 ppm (by K.F.) obtained from Energy Chemical. Flash column chromatography was performed using silica gel 60 (100-200 mesh). Analytical thin layer chromatography (TLC) was carried out on Huanghai Chromatography silica gel plate HSGF254 indicator and visualized by UV. The purity ($\geqslant$95%) of the compounds was verified by the HPLC study performed on Agilent C18 (4.6 mm × 150 mm, 3.5 μm) column

using a mixture of solvent methanol/water at a flow rate of 1.0 mL/min. The ^{1}H NMR spectra were measured on a Bruker AV-300 instrument using deuterated solvents with tetramethylsilane (TMS) as internal standard. ESI-mass and high-resolution mass spectra (HRMS) were recorded on a Water Q-Tof micro mass spectrometer.

methyl (*E*)-4-((4-hydroxyphenyl)diazenyl)benzoate (3). The suspension of compound 2 (11.54 g, 76.1 mmol) in water (135 ml) was cooled to 5℃ and HCl (15.8 ml, 190 mmol) was added to the mixture. To the mixture was added the cooled (5℃) solution of sodium nitrate (5.03 g, 79.8 mmol) in water (35 ml) and stirred at 5℃. After 1h, the solution of phenol (1) (7.52 g, 79.9 mmol), K_2CO_3 (15.0 g, 108.5 mmol) in water (120 ml) dropwised to the reaction mixture for 10 min and stirred at room temperature for 3h. After the reaction was completed, dilute acetic acid was added to the mixture and adjusted to pH = 4.0. The product was filtered, and washed with water, methanol to give compound 3 (15.65 g, 80.3%) in a brown solid. ^{1}H NMR (300 MHz, DMSO-d_6) δ 10.57 (s, 1H), 8.18 – 8.09 (m, 2H), 7.96 – 7.80 (m, 4H), 6.97 (d, J = 8.4 Hz, 2H), 3.89 (s, 3H).

General Procedures for the Synthesis of Intermediates 4a-4e. Stir a solution of methyl (E)-4-((4-hydroxyphenyl)diazenyl)benzoate (**3**) (2.56 g, 10 mmol), 1-bromo-n-chlorohydrocarbon (12 mmol, 1.2 eq) and potassium carbonate (4.14 g, 30 mmol), in *N,N*-dimethylforamide (20 mL) under room temperature for 20 hours. 200 mL water was added to the mixture with stirring. The product was filtered, then washed with water and dry in 60℃ to give compound **4** in a yellow solid.

methyl (*E*)-4-((4-(2-chloroethoxy)phenyl)diazenyl)benzoate (4a). ^{1}H NMR (300 MHz, DMSO-d_6) δ 8.22 – 8.06 (m, 2H), 7.98 – 7.81 (m, 4H), 7.29 – 7.09 (m, 2H), 4.38 (t, J = 11.2 Hz, 2H), 4.08 – 3.94 (m, 2H), 3.90 (s, 3H).

methyl (*E*)-4-((4-(3-chloropropoxy)phenyl)diazenyl)benzoate (4b). ^{1}H NMR (300 MHz, Chloroform-d) δ 8.24 – 8.12 (m, 2H), 8.01 – 7.86 (m, 4H), 7.09 – 6.97 (m, 2H), 4.21 (t, *J* = 5.8 Hz, 2H), 3.95 (s, 3H), 3.77 (t, *J* = 6.2 Hz, 2H), 2.28 (p, *J* = 6.0 Hz, 2H).

methyl (*E*)-4-((4-(4-chlorobutoxy)phenyl)diazenyl)benzoate(4c). ^{1}H NMR (300 MHz, Chloroform-d) δ 8.17 (d, *J* = 8.3 Hz, 2H), 7.92 (dd, *J* = 11.4, 8.5 Hz, 4H), 7.01 (d, *J* = 8.5 Hz, 2H), 4.09 (d, *J* = 5.2 Hz, 2H), 3.95 (s, 3H), 3.63 (d, *J* = 5.9 Hz, 2H), 2.01 (p, *J* = 2.9 Hz, 4H).

methyl (*E*)-4-((4-((5-chloropentyl)oxy)phenyl)diazenyl)benzoate(4d). ^{1}H NMR (300 MHz, Chloroform-d) δ 8.17 (d, *J* = 8.4 Hz, 2H), 7.99 – 7.85 (m, 4H), 7.06 – 6.96 (m, 2H), 4.07 (t, *J* = 6.3 Hz, 2H), 3.95 (s, 3H), 3.59 (t, *J* = 6.6 Hz, 2H), 1.95 – 1.80 (m, 4H), 1.66 (ddt, *J* = 14.5, 9.7, 5.7 Hz, 2H).

methyl (*E*)-4-((4-((6-chlorohexyl)oxy)phenyl)diazenyl)benzoate (4e). ^{1}H NMR (300 MHz, DMSO-d_6) δ 8.15 (d, *J* = 8.0 Hz, 2H), 7.93 (d, *J* = 8.2 Hz, 4H), 7.15 (d, *J* = 8.4 Hz, 2H), 4.17 – 4.05 (m, 2H), 3.90 (s, 3H), 3.65 (t, *J* = 5.8 Hz, 2H), 1.84 – 1.66 (m, 4H), 1.56 – 1.38 (m, 4H).

General Procedures for the Synthesis of Intermediates 5a-5e. Stir a solution of methyl compound 4 (5 mmol), lithium hydroxide (600 mg, 25 mmol) in water and Tetrahydrofuran (1:1, 20 mL) under room temperature overnight. 200 mL water was added to the mixture with stirring, and then dilute hydrochloric acid was added and adjusted to pH = 2. The product was filtered, then washed with water and dry in 60℃ to give compound 5 in orange solid.

(*E*)-4-((4-(2-chloroethoxy)phenyl)diazenyl)benzoic acid (5a). ^{1}H NMR (300 MHz, DMSO-d_6) δ 13.40 – 12.80 (s, 1H), 8.32 – 8.10 (m, 2H), 8.06 – 7.81 (m, 4H), 7.29 – 7.09 (m, 2H), 4.38 (t, *J* = 10.8 Hz, 2H), 4.12 – 3.92 (m, 2H).

(*E*)-4-((4-(3-chloropropoxy)phenyl)diazenyl)benzoic acid (5b). ^{1}H NMR (300 MHz, DMSO-d_6) δ 8.06 (d, *J* = 8.1 Hz, 2H), 7.90 (d, *J* = 8.5 Hz, 2H), 7.78 (d, *J* = 8.1 Hz, 2H), 7.16 (d, *J* = 8.5 Hz, 2H), 5.76 (s, 2H), 4.21 (t, *J* = 6.1 Hz, 2H), 3.82 (t, *J* = 6.5 Hz, 2H), 2.22 (p, *J* = 6.4 Hz, 2H).

(*E*)-4-((4-(4-chlorobutoxy)phenyl)diazenyl)benzoic acid (5c). ^{1}H NMR (300 MHz, DMSO-d_6) δ 8.04 (d, *J* = 8.0 Hz, 2H), 7.90 (d, *J* = 8.6 Hz, 2H), 7.78 (d, *J* = 8.1 Hz, 2H), 7.14 (d, *J* = 8.5 Hz, 2H), 4.13 (d, *J* = 5.2 Hz, 2H), 1.97 – 1.77 (m, 4H).

(*E*)-4-((4-((5-chloropentyl)oxy)phenyl)diazenyl)benzoic acid (5d). ^{1}H NMR (300 MHz, DMSO-d_6) δ 8.09 (d, *J* = 8.0 Hz, 2H), 7.86 (dd, *J* = 25.2, 8.2 Hz, 4H), 7.13 (d, *J* = 8.5 Hz, 2H), 4.10 (t, *J* = 6.4 Hz, 2H), 3.68 (d, *J* = 13.2 Hz, 2H), 1.79 (dq, *J* = 12.5, 5.6 Hz, 4H), 1.57 (q, *J* = 7.9 Hz, 2H).

(*E*)-4-((4-((6-chlorohexyl)oxy)phenyl)diazenyl)benzoic acid (5e). ^{1}H NMR (300 MHz, DMSO-d_6) δ 8.04 (d, *J* = 7.9 Hz, 2H), 7.88 (d, *J* = 8.4 Hz, 2H), 7.77 (d, *J* = 7.9 Hz, 2H), 7.12 (d, *J* = 8.5 Hz, 2H), 4.07 (d, *J* = 6.6 Hz, 2H), 3.64 (t, *J* = 6.7 Hz, 2H), 1.88 – 1.62 (m, 4H), 1.57 – 1.31 (m, 4H).

General Procedures for the Synthesis of Intermediates 6a-6e. Stir a solution of compound **5** (2.0 mmol), oxalyl chloride (338 μL, 4.0 mmol) in 10mL extra dry THF under room temperature, then add one drop of *N,N*-Dimethylformamide as catalyst and stir for 30 min at room temperature. The solvent was evaporated to dry, then the mixture was re-dissolved with 5mL extra dry THF and added to the solution of lenalidomide and DIEA in extra dry THF dropwise with stirring. After the reaction completely, the solvent was evaporated to dry, and the mixture was recrystallized with methanol to get compound **6** in orange solid.

(*E*)-4-((4-(2-chloroethoxy)phenyl)diazenyl)-N-(2-(2,6-dioxopiperidin-3-yl)-1-oxoisoindolin-4-yl)benzamide (6a). ^{1}H NMR (300 MHz, DMSO-d_6) δ 10.96 (s, 1H), 10.48 (s, 1H), 8.18 (d, *J* = 8.2 Hz, 2H), 7.96 (dt, *J* = 8.9, 4.2 Hz, 4H), 7.76 (d, *J* = 7.5 Hz, 1H), 7.65 – 7.55 (m, 2H), 7.26 – 7.14 (m, 2H), 5.15 (dd, *J* = 13.2, 5.2 Hz, 1H), 4.47 (d, *J* = 2.6 Hz, 2H), 4.40 (t, *J* = 5.1 Hz, 2H), 4.00 (t, *J* = 5.1 Hz, 2H), 2.99 – 2.81 (m, 1H), 2.67 – 2.54 (m, 1H), 2.45 – 2.27 (m, 1H), 2.07 – 1.93 (m, 1H). ESI-HRMS: calcd for $C_{28}H_{24}ClN_5O_5$, 545.1466; m/z: $[M]^+$= 546.15387.

(*E*)-4-((4-(3-chloropropoxy)phenyl)diazenyl)-N-(2-(2,6-dioxopiperidin-3-yl)-1-oxoisoindolin-4-yl)benzamide (6b). ^{1}H NMR (300 MHz, DMSO-d_6) δ 10.99 (s, 1H), 10.51 (s, 1H), 8.19 (d, *J* = 8.2 Hz, 2H), 7.97 (dd, *J* = 8.4, 5.8 Hz, 4H), 7.77 (d, *J* = 7.5 Hz, 1H), 7.60 (dt, *J* = 15.2, 7.5 Hz, 2H), 7.19 (d, *J* = 8.6 Hz, 2H), 5.17 (dd, *J* = 13.2, 5.0 Hz, 1H), 4.54 – 4.38 (m, 2H), 4.23 (t, *J* = 6.0 Hz, 2H), 3.83 (t, *J* = 6.5 Hz, 2H), 2.99 – 2.82 (m, 1H), 2.64 – 2.54 (m, 1H), 2.45 – 2.34 (m, 1H), 2.23 (p, J = 6.5 Hz, 2H), 2.04 – 1.97 (m, 1H). ESI-HRMS: calcd for $C_{29}H_{26}ClN_5O_5$, 559.1622; m/z: $[M]^+$= 560.16952.

(*E*)-4-((4-(4-chlorobutoxy)phenyl)diazenyl)-N-(2-(2,6-dioxopiperidin-3-yl)-1-oxoisoindolin-4-yl)benzamide (6c). ^{1}H NMR (300 MHz, DMSO- d_6) δ 11.01 (s, 1H), 10.53 (s, 1H), 8.15 (dd, *J* = 18.7, 8.2 Hz, 2H), 7.94 (dd, *J* = 11.3, 8.3 Hz, 4H), 7.77 (d, *J* = 7.4 Hz, 1H), 7.60 (dt, *J* = 14.9, 7.4 Hz, 2H), 7.16 (dd, *J* = 9.2, 2.8 Hz, 2H), 5.17 (dd, *J* = 13.5, 4.9 Hz, 1H), 4.47 (s, 2H), 4.15 (s, 2H), 3.73 (d, *J* = 6.5 Hz, 2H), 2.99 – 2.85 (m, 1H), 2.66 – 2.55 (m, 1H), 2.48 – 2.33 (m, 1H), 2.07 – 1.98 (m, 1H), 1.96 – 1.79 (m, 4H). MS(ESI): calcd for $C_{30}H_{28}ClN_5O_5$, 573.1779; m/z: $[M]^+$= 574.18517.

(*E*)-4-((4-((5-chloropentyl)oxy)phenyl)diazenyl)-N-(2-(2,6-dioxopiperidin-3-yl)-1-oxoisoindolin-4-yl)benzamide (6d). ^{1}H NMR (300 MHz, DMSO- d_6) δ 10.90 (s, 1H), 10.42 (s,

1H), 8.09 (d, *J* = 8.2 Hz, 2H), 7.87 (t, *J* = 7.9 Hz, 4H), 7.67 (d, *J* = 7.5 Hz, 1H), 7.51 (dt, *J* = 15.1, 7.5 Hz, 2H), 7.07 (d, *J* = 8.5 Hz, 2H), 5.07 (dd, *J* = 13.1, 5.2 Hz, 1H), 4.43 – 4.33 (m, 2H), 4.03 (t, *J* = 6.3 Hz, 2H), 3.59 (t, *J* = 6.5 Hz, 2H), 2.90 – 2.80 (m, 1H), 2.62 – 2.48 (m, 1H), 2.46 – 2.32 (m, 1H), 1.99 – 1.87 (m, 1H), 1.70 (d, *J* = 9.7 Hz, 4H), 1.47 (t, *J* = 7.8 Hz, 2H). ESI-HRMS: calcd for $C_{31}H_{30}ClN_5O_5$, 587.1935; m/z: $[M]^+$= 588.20082.

(*E*)-4-((4-((6-chlorohexyl)oxy)phenyl)diazenyl)-N-(2-(2,6-dioxopiperidin-3-yl)-1-oxoisoindolin-4-yl)benzamide (6e). ^{1}H NMR (300 MHz, DMSO-d_6) δ 11.00 (s, 1H), 10.52 (s, 1H), 8.18 (d, *J* = 8.3 Hz, 2H), 7.95 (t, *J* = 8.2 Hz, 4H), 7.76 (d, *J* = 7.4 Hz, 1H), 7.60 (dt, *J* = 15.0, 7.4 Hz, 2H), 7.15 (d, *J* = 8.6 Hz, 2H), 5.16 (dd, *J* = 13.1, 5.1 Hz, 1H), 4.54 – 4.40 (m, 2H), 4.10 (t, *J* = 6.5 Hz, 2H), 3.65 (t, *J* = 6.6 Hz, 2H), 2.96 – 2.84 (m, 1H), 2.68 – 2.52 (m, 1H), 2.46 – 2.33 (m, 1H), 2.04 – 1.98 (m, 1H), 1.88 – 1.62 (m, 4H), 1.47 (d, *J* = 7.1 Hz, 4H). ESI-HRMS: calcd for $C_{32}H_{32}ClN_5O_5$, 601.2092; m/z: $[M]^+$= 602.21647.

N-(2-Chloro-6-methylphenyl)-2-(2-methyl-6-(piperazin-1-yl)pyrimidin-4-ylamino)thiazole-5-carboxamide (8). 2-(6-Chloro-2-methylpyrimidin-4-ylamino)-N-(2-chloro-6-methylphenyl)thiazole-5-carboxamide, **7** (1.00 g, 2.54 mmol), piperazine (2.19 g, 25.4 mmol), and N,N-diisopropylethylamine (0.84 mL, 5.07 mmol) were dissolved in 30 mL of extra dry 1,4-dioxane and refluxed overnight. The solvent was stripped and the residue was triturated several times with water/MeOH, MeOH/ether, and then ether. The white solid was dried under high vacuum to give precursor 4 (0.82 g, 73%). ^{1}H NMR (300 MHz, DMSO-d6) δ 9.88 (s, 1H), 8.21 (s, 1H), 7.40 (d, *J* = 7.3 Hz, 1H), 7.26 (d, J = 8.2 Hz, 2H), 6.02 (s, 1H), 3.48 – 3.37 (m, 4H), 2.78 – 2.70 (m, 4H), 2.40 (s, 3H), 2.23 (s, 3H).

General Procedures for the Synthesis of Intermediates 9a-9e. To a solution of 6 (0.11 mmol) in Acetone (10 ml) was added NaI (83mg, 0.55 mmol). The reaction mixture was stirred at reflux temperature for 24 h, then remove Acetone by vacuum. Add **8** (43 mg, 0.10 mmol), DIEA (96 μL, 0.57 mmol) in DMF (1 ml) and the resulting solution stirred for 16 h at 80 °C. Then the mixture was cooled down to rt. The solvent was evaporated, and the residue subjected to Prep TLC purification (MeOH/DCM from1/50 to 1/25) to give the desired product as orange solid.

(*E*)-N-(2-chloro-6-methylphenyl)-2-((6-(4-(2-(4-((4-((2-(2,6-dioxopiperidin-3-yl)-1-oxoisoindolin-4-yl)carbamoyl)phenyl)diazenyl)phenoxy)ethyl)piperazin-1-yl)-2-methylpyrimidin-4-yl)amino)thiazole-5-carboxamide (9a). ^{1}H NMR (300 MHz, DMSO-d_6) δ 11.47 (s, 1H), 10.99 (s, 1H), 10.51 (s, 1H), 9.87 (s, 1H), 8.26 – 8.13 (m, 3H), 8.06 – 7.85 (m, 4H), 7.75 (d, *J* = 7.4 Hz, 1H), 7.68 – 7.46 (m, 2H), 7.38 (d, *J* = 7.4 Hz, 1H), 7.32 – 7.15 (m, 4H), 6.05 (s, 1H), 5.15 (dd, J = 13.2, 5.2 Hz, 1H), 4.43 (d, *J* = 16.4 Hz, 2H), 4.25 (d, *J* = 5.1 Hz, 2H), 3.59 – 3.46 (m, 4H), 2.99 – 2.88 (m, 1H), 2.77 – 2.67 (m, 1H), 2.63 – 2.53 (m, 4H), 2.40 (s, 3H), 2.36 – 2.30 (m, 1H), 2.22 (s, 3H), 2.06 – 1.91 (m, 1H). ESI-HRMS: calcd for $C_{48}H_{45}ClN_{12}O_6S$, 952.2994; m/z: $[M]^+$= 953.3036. Purity: 96.77% by HPLC (MeCN/H_2O =70:30).

(*E*)-N-(2-chloro-6-methylphenyl)-2-((6-(4-(3-(4-((4-((2-(2,6-dioxopiperidin-3-yl)-1-oxoisoindolin-4-yl)carbamoyl)phenyl)diazenyl)phenoxy)propyl)piperazin-1-yl)-2-methylpyrimidin-4-yl)amino)thiazole-5-carboxamide (9b). ^{1}H NMR (300 MHz, DMSO-d_6) δ 11.47 (s, 1H), 10.99 (s, 1H), 10.51 (s, 1H), 9.87 (s, 1H), 8.25 – 8.11 (m, 3H), 7.95 (dd, *J* = 8.5, 5.9 Hz, 4H), 7.75 (d, *J* = 7.4 Hz, 1H), 7.60 (dd, *J* = 13.7, 7.4 Hz, 2H), 7.38 (dd, *J* = 7.3, 2.1 Hz, 1H), 7.31 – 7.12 (m, 4H), 6.04 (s, 1H), 5.15 (dd, *J* = 13.2, 5.2 Hz, 1H), 4.46 (s, 2H), 4.23 – 4.12 (m, 2H), 3.59 – 3.46 (m, 4H), 2.96 – 2.85 (m, 1H), 2.63 – 2.60 (m, 1H), 2.57 – 2.49 (m, 4H), 2.39 (s,

3H), 2.32 – 2.25 (m, 1H), 2.22 (s, 3H), 2.07 – 1.88 (m, 3H). ESI-HRMS: calcd for $C_{49}H_{47}ClN_{12}O_6S$, 966.3251; m/z $[M]^+$= 967.3325. Purity: 98.85% by HPLC (MeCN/H_2O =70:30).

(E)-N-(2-chloro-6-methylphenyl)-2-((6-(4-(4-(4-(4-((4-((2-(2,6-dioxopiperidin-3-yl)-1-oxoisoindolin-4-yl)carbamoyl)phenyl)diazenyl)phenoxy)butyl)piperazin-1-yl)-2-methylpyrimidin-4-yl)amino)thiazole-5-carboxamide (9c). ^{1}H NMR (300 MHz, DMSO-d_6) δ 11.41 (s, 1H), 10.96 (s, 1H), 10.44 (d, *J* = 15.3 Hz, 1H), 9.83 (s, 1H), 8.30 – 8.09 (m, 3H), 7.95 (t, *J* = 7.4 Hz, 4H), 7.80 (dd, *J* = 18.2, 7.5 Hz, 1H), 7.58 (h, *J* = 8.5, 7.9 Hz, 3H), 7.38 (d, *J* = 7.4 Hz, 1H), 7.25 (d, *J* = 8.2 Hz, 2H), 7.16 (d, *J* = 8.8 Hz, 2H), 6.05 (d, *J* = 6.7 Hz, 1H), 5.15 (dd, *J* = 13.6, 5.2 Hz, 1H), 4.50 (d, *J* = 17.5 Hz, 2H), 4.13 (d, *J* = 6.6 Hz, 2H), 3.55 – 3.49 (m, 4H), 3.05 – 2.79 (m, 1H), 2.66 – 2.54 (m, 1H), 2.44 (s, 3H), 2.43 – 2.33 (m, 4H), 2.32 – 2.26 (m, 1H), 2.25 – 2.19 (s, 3H), 2.10 – 1.95 (m, 1H), 1.89 – 1.71 (m, 2H), 1.63 (t, *J* = 7.9 Hz, 2H). MS(ESI): calcd for $C_{50}H_{49}ClN_{12}O_6S$, 980.3307; m/z: $[M]^+$= 981.33728**.** Purity: 96.20% by HPLC (MeCN/H_2O =70:30).

(*E*)-N-(2-chloro-6-methylphenyl)-2-((6-(4-(5-(4-((4-((2-(2,6-dioxopiperidin-3-yl)-1-oxoisoindolin-4-yl)carbamoyl)phenyl)diazenyl)phenoxy)pentyl)piperazin-1-yl)-2-methylpyrimidin-4-yl)amino)thiazole-5-carboxamide (9d). ^{1}H NMR (300 MHz, DMSO-d_6) δ 11.46 (s, 1H), 10.99 (s, 1H), 10.51 (s, 1H), 9.86 (s, 1H), 8.25 – 8.12 (m, 3H), 7.95 (t, *J* = 7.7 Hz, 4H), 7.75 (d, *J* = 7.4 Hz, 1H), 7.60 (dd, *J* = 13.6, 7.2 Hz, 2H), 7.38 (d, *J* = 7.4 Hz, 1H), 7.25 (d, *J* = 7.9 Hz, 2H), 7.15 (d, *J* = 8.6 Hz, 2H), 6.03 (s, 1H), 5.15 (dd, *J* = 12.2, 5.2 Hz, 1H), 4.50 – 4.37 (m, 2H), 4.09 (d, *J* = 6.7 Hz, 2H), 3.60 – 3.41 (m, 4H), 2.98 – 2.82 (m, 1H), 2.64 – 2.53 (m, 1H), 2.42 (s, 3H), 2.41 – 2.34(m, 4H), 2.33 – 2.27 (m, 1H), 2.22 (s, 3H), 2.01 – 1.94 (m, 1H), 1.85 – 1.70 (m, 2H), 1.57 – 1.43 (s, 4H). MS(ESI): calcd for $C_{51}H_{51}ClN_{12}O_6S$ 994.3464; m/z: $[M]^+$=995.3535**.** Purity: 99.13% by HPLC (MeCN/H_2O =70:30).

(*E*)-N-(2-chloro-6-methylphenyl)-2-((6-(4-(6-(4-((4-((2-(2,6-dioxopiperidin-3-yl)-1-oxoisoindolin-4-yl)carbamoyl)phenyl)diazenyl)phenoxy)hexyl)piperazin-1-yl)-2-methylpyrimidin-4-yl)amino)thiazole-5-carboxamide (9e). ^{1}H NMR (300 MHz, DMSO-d_6) δ 11.39 (s, 1H), 10.92 (s, 1H), 10.41 (s, 1H), 9.80 (s, 1H), 8.25 – 8.02 (m, 3H), 7.90 (t, *J* = 8.1 Hz, 4H), 7.73 (p, *J* = 10.2, 8.7 Hz, 1H), 7.54 (dt, *J* = 15.6, 7.8 Hz, 2H), 7.34 (d, *J* = 7.3 Hz, 1H), 7.20 (d, *J* = 8.3 Hz, 2H), 7.09 (d, *J* = 8.6 Hz, 2H), 6.00 (s, 1H), 5.11 (dd, *J* = 13.1, 5.2 Hz, 1H), 4.50 – 4.34 (m, 2H), 4.04 (t, *J* = 6.4 Hz, 2H), 3.46 (d, *J* = 6.7 Hz, 4H), 2.96 – 2.78 (m, 1H), 2.61 – 2.53 (m, 1H), 2.41 – 2.31 (m, 4H), 2.26 (s, 3H), 2.21 – 2.11 (m, 4H), 2.01 – 1.87 (m, 1H), 1.79 – 1.64 (m, 2H), 1.42 (q, *J* = 7.1 Hz, 4H), 1.34 (d, *J* = 9.6 Hz, 2H). MS (ESI):calcd for $C_{52}H_{53}ClN_{12}O_6S$ 1008.3620; m/z: $[M]^+$= 1009.36956. Purity: 95.51% by HPLC (MeCN/H_2O =70:30).

Tert-butyl (2-(2,6-dioxopiperidin-3-yl)-1-oxoisoindolin-4-yl)carbamate (11). ^{1}H NMR (300 MHz, DMSO-d_6) δ 11.04 (s, 1H), 9.26 (s, 1H), 7.80 (dd, *J* = 6.3, 2.4 Hz, 1H), 7.51 – 7.41 (m, 2H), 5.16 (dd, *J* = 13.2, 5.0 Hz, 1H), 4.51 – 4.32 (m, 2H), 2.94 (d, *J* = 7.5 Hz, 1H), 2.68 (s, 1H), 2.38 (tt, *J* = 13.2, 6.7 Hz, 1H), 2.08 (s, 1H), 1.52 (s, 9H).

Tert-butyl (2-(1-methyl-2,6-dioxopiperidin-3-yl)-1-oxoisoindolin-4-yl)carbamate (12). ^{1}H NMR (300 MHz, DMSO-d_6) δ 9.24 (s, 1H), 7.78 (s, 1H), 7.48 (s, 2H), 5.21 (dd, *J* = 12.9, 4.3 Hz, 1H), 4.56 – 4.25 (m, 2H), 3.04 (s, 3H), 2.98 (s, 1H), 2.79 (d, *J* = 18.5 Hz, 1H), 2.48 – 2.29 (m, 1H), 2.05 (d, *J* = 19.3 Hz, 1H), 1.51 (s, 9H).

(*E*)-4-((4-(4-chlorobutoxy)phenyl)diazenyl)-N-(2-(2,6-dioxopiperidin-3-yl)-1-oxoisoindolin-4-yl)benzamide (13). ^{1}H NMR (300 MHz, DMSO-d_6) δ 10.59 (s, 1H), 8.21 (d, *J* = 8.2 Hz, 2H), 7.99 (t, *J* = 8.1 Hz, 4H), 7.79 (d, *J* = 7.5 Hz, 1H), 7.71 – 7.60 (m, 2H), 7.20 (d, *J* = 8.6 Hz, 2H), 5.28 (dd, *J* = 13.4, 5.1 Hz, 1H), 4.60 – 4.38 (m, 2H), 4.19 (d, *J* = 5.6 Hz, 2H), 3.76

(q, J = 10.5, 8.0 Hz, 2H), 2.97 (d, J = 5.0 Hz, 1H), 2.77 (d, J = 16.8 Hz, 1H), 2.43 (q, J = 12.2, 8.3 Hz, 1H), 2.10 – 2.00 (m, 1H), 1.97 – 1.85 (m, 4H). ESI-HRMS: calcd for $C_{31}H_{30}ClN_5O_5$, 587.1935; m/z: $[M]^+$= 588.20082.

(*E*)-N-(2-chloro-6-methylphenyl)-2-((2-methyl-6-(4-(4-(4-((4-((2-(1-methyl-2,6-dioxopiperidin-3-yl)-1-oxoisoindolin-4-yl)carbamoyl)phenyl)diazenyl)phenoxy)butyl)piperazin-1-yl)pyrimidin-4-yl)amino)thiazole-5-carboxamide (14). 1H NMR (300 MHz, DMSO-d_6) δ 11.53 (s, 1H), 10.58 (s, 1H), 9.92 (s, 1H), 8.29 – 8.17 (m, 3H), 8.00 (dd, J = 8.6, 6.5 Hz, 5H), 7.79 (d, J = 7.5 Hz, 1H), 7.71 – 7.60 (m, 2H), 7.43 (dd, J = 7.3, 2.3 Hz, 1H), 7.30 (t, J = 4.8 Hz, 2H), 7.20 (d, J = 8.7 Hz, 2H), 6.09 (s, 1H), 5.28 (dd, J = 13.5, 5.1 Hz, 1H), 4.61 – 4.39 (m, 2H), 4.18 (t, J = 6.4 Hz, 2H), 3.56 (s, 4H), 3.04 (s, 4H), 2.77 (d, J = 16.2 Hz, 1H), 2.47 (s, 3H), 2.44 (s, 4H), 2.27 (s, 3H), 2.10 – 2.01 (m, 1H), 1.83 (d, J = 7.6 Hz, 2H), 1.69 (s, 2H). ESI-HRMS: calcd for $C_{51}H_{51}ClN_{12}O_6S$, 994.3464; m/z: $[M]^+$= 995.35365. Purity: 96.28 % by HPLC (MeCN/H_2O =80:20).

ASSOCIATED CONTENT

Supporting Information.

SI-Experimental section, NMR spectra and HPLC traces (PDF)

SI-Comma delimited.csv (CSV)

AUTHOR INFORMATION

Corresponding Author

* youqd@163.com

* jiangzhengyucpu@163.com

Author Contributions

‡Yu-Hui Jin and Meng-Chen Lu contributed equally.

Notes

The authors declare no competing financial interests.

Funding Sources

This study was supported by projects, [81773581], [81773639], [81803363] and [81930100] of the National Natural Science Foundation of China; [BK20160746] of the Natural Science Foundation of Jiangsu Province of China; [CPU2018GY02] of Double First Class Innovation Team of China Pharmaceutical University; National Science & Technology Major Project 'Key New Drug Creation and Manufacturing Program', China(No: 2018ZX09711002); China Postdoctoral Science Foundation-funded Project (1600010006 and 2018T110576);The Program for Outstanding Scientific and Technological Innovation Team of Jiangsu Higher Education; the "Qing Lan" Project of Jiangsu Province and the Young Elite Scientists Sponsorship Program by CAST.

ABBREVIATIONS

PROTACs, Proteolysis-Targeting Chimeras; CRISPR, Clustered regularly interspaced short palindromic repeats; HyTs, Hydrophobic Tags.

REFERENCES

1. Daniel, K.; Icha, J.; Horenburg, C.; Muller, D.; Norden, C.; Mansfeld, J. Conditional Control of Fluorescent Protein Degradation by an Auxin-Dependent Nanobody. *Nat. Commun.* **2018,** *9*, 3297.

2. Clift, D.; McEwan, W. A.; Labzin, L. I.; Konieczny, V.; Mogessie, B.; James, L. C.; Schuh, M. A Method for the Acute and Rapid Degradation of Endogenous Proteins. *Cell* **2017,** *171*, 1692-1706.

3. Fan, X.; Jin, W. Y.; Lu, J.; Wang, J.; Wang, Y. T. Rapid and Reversible Knockdown of Endogenous Proteins by Peptide-Directed Lysosomal Degradation. *Nat. Neurosci.* **2014,** *17*, 471-480.

4. Elbashir, S. M.; Harborth, J.; Lendeckel, W.; Yalcin, A.; Weber, K.; Tuschl, T. Duplexes of 21-Nucleotide RNAs Mediate RNA Interference in Cultured Mammalian Cells. *Nature* **2001,** *411*, 494-498.

5. Lai, A. C.; Crews, C. M. Induced Protein Degradation: An Emerging Drug Discovery Paradigm. *Nat. Rev. Drug. Discov.* **2017,** *16*, 101-114.

6. Sun, Y.; Zhao, X.; Ding, N.; Gao, H.; Wu, Y.; Yang, Y.; Zhao, M.; Hwang, J.; Song, Y.; Liu, W.; Rao, Y. PROTAC-Induced BTK Degradation as a Novel Therapy for Mutated BTK C481s Induced Ibrutinib-Resistant B-Cell Malignancies. *Cell. Res.* **2018,** *28*, 779-781.

7. Gadd, M. S.; Testa, A.; Lucas, X.; Chan, K. H.; Chen, W.; Lamont, D. J.; Zengerle, M.; Ciulli, A. Structural Basis of PROTAC Cooperative Recognition for Selective Protein Degradation. *Nat. Chem. Biol.* **2017,** *13*, 514-521.

8. Powell, C. E.; Gao, Y.; Tan, L.; Donovan, K. A.; Nowak, R. P.; Loehr, A.; Bahcall, M.; Fischer, E. S.; Janne, P. A.; George, R. E.; Gray, N. S. Chemically Induced Degradation of Anaplastic Lymphoma Kinase (ALK). *J. Med. Chem.* **2018,** *61*, 4249-4255.

9. Neklesa, T. K.; Tae, H. S.; Schneekloth, A. R.; Stulberg, M. J.; Corson, T. W.; Sundberg, T. B.; Raina, K.; Holley, S. A.; Crews, C. M. Small-Molecule Hydrophobic Tagging-Induced Degradation of Halotag Fusion Proteins. *Nat. Chem. Biol.* **2011,** *7*, 538-543.

10. Beharry, A. A.; Woolley, G. A. Azobenzene Photoswitches for Biomolecules. *Chem. Soc. Rev.* **2011,** *40*, 4422-4437.

11. Pfaff, P.; Samarasinghe, K. T. G.; Crews, C. M.; Carreira, E. M. Reversible Spatiotemporal Control of Induced Protein Degradation by Bistable Photoprotacs. *ACS. Cent. Sci.* **2019,** *5*, 1682-1690.

12. Delacour, Q.; Li, C.; Plamont, M. A.; Billon-Denis, E.; Aujard, I.; Le Saux, T.; Jullien, L.; Gautier, A. Light-Activated Proteolysis for the Spatiotemporal Control of Proteins. *ACS. Chem. Biol.* **2015,** *10*, 1643-1647.

13. Mills, E.; Truong, K. Photoswitchable Protein Degradation: A Generalizable Control Module for Cellular Function? *Chem. Biol.* **2013,** *20*, 458-460.

14. Renicke, C.; Schuster, D.; Usherenko, S.; Essen, L. O.; Taxis, C. A LOV2 Domain-Based Optogenetic Tool to Control Protein Degradation and Cellular Function. *Chem. Biol.* **2013,** *20*, 619-626.

15. Scheffer, J.; Hasenjager, S.; Taxis, C. Degradation of Integral Membrane Proteins Modified with the Photosensitive Degron Module Requires the Cytosolic Endoplasmic Reticulum-Associated Degradation Pathway. *Mol. Biol. Cell.* **2019,** *30*, 2558-2570.

16. Taxis, C. Development of a Synthetic Switch to Control Protein Stability in Eukaryotic Cells with Light. *Methods. Mol. Biol.* **2017,** *1596*, 241-255.

17. Akinboye, E. S.; Rosen, M. D.; Denmeade, S. R.; Kwabi-Addo, B.; Bakare, O. Design, Synthesis, and Evaluation of Ph-Dependent Hydrolyzable Emetine Analogues as Treatment for Prostate Cancer. *J. Med. Chem.* **2012,** *55*, 7450-7459.

18. Hansen, M. J.; Feringa, F. M.; Kobauri, P.; Szymanski, W.; Medema, R. H.; Feringa, B. L. Photoactivation of MDM2 Inhibitors: Controlling Protein-Protein Interaction with Light. *J. Am. Chem. Soc.* **2018,** *140*, 13136-13141.

19. Legigan, T.; Clarhaut, J.; Renoux, B.; Tranoy-Opalinski, I.; Monvoisin, A.; Berjeaud, J. M.; Guilhot, F.; Papot, S. Synthesis and Antitumor Efficacy of a Beta-Glucuronidase-Responsive Albumin-Binding Prodrug of Doxorubicin. *J. Med. Chem.* **2012,** *55*, 4516-4520.

20. Sakabe, M.; Asanuma, D.; Kamiya, M.; Iwatate, R. J.; Hanaoka, K.; Terai, T.; Nagano, T.; Urano, Y. Rational Design of Highly Sensitive Fluorescence Probes for Protease and Glycosidase Based on Precisely Controlled Spirocyclization. *J. Am. Chem. Soc.* **2013,** *135*, 409-414.

21. Wu, X.; Sun, X.; Guo, Z.; Tang, J.; Shen, Y.; James, T. D.; Tian, H.; Zhu, W. In Vivo and in Situ Tracking Cancer Chemotherapy by Highly Photostable Nir Fluorescent Theranostic Prodrug. *J. Am. Chem. Soc.* **2014,** *136*, 3579-3588.

22. Jia, C.; Migliore, A.; Xin, N.; Huang, S.; Wang, J.; Yang, Q.; Wang, S.; Chen, H.; Wang, D.; Feng, B.; Liu, Z.; Zhang, G.; Qu, D. H.; Tian, H.; Ratner, M. A.; Xu, H. Q.; Nitzan, A.; Guo, X. Covalently Bonded Single-Molecule Junctions with Stable and Reversible Photoswitched Conductivity. *Science* **2016,** *352*, 1443-1445.

23. Mogaki, R.; Okuro, K.; Aida, T. Adhesive Photoswitch: Selective Photochemical Modulation of Enzymes under Physiological Conditions. *J. Am. Chem. Soc.* **2017,** *139*, 10072-10078.

24. Mourot, A.; Fehrentz, T.; Le Feuvre, Y.; Smith, C. M.; Herold, C.; Dalkara, D.; Nagy, F.; Trauner, D.; Kramer, R. H. Rapid Optical Control of Nociception with an Ion-Channel Photoswitch. *Nat. Methods.* **2012,** *9*, 396-402.

25. Velema, W. A.; Szymanski, W.; Feringa, B. L. Photopharmacology: Beyond Proof of Principle. *J. Am. Chem. Soc.* **2014,** *136*, 2178-2191.

26. Hull, K.; Morstein, J.; Trauner, D. In Vivo Photopharmacology. *Chem. Rev.* **2018,** *118*, 10710-10747.

27. Agnetta, L.; Kauk, M.; Canizal, M. C. A.; Messerer, R.; Holzgrabe, U.; Hoffmann, C.; Decker, M. A Photoswitchable Dualsteric Ligand Controlling Receptor Efficacy. *Angew. Chem. Int. Ed. Engl.* **2017,** *56*, 7282-7287.

28. Broichhagen, J.; Podewin, T.; Meyer-Berg, H.; von Ohlen, Y.; Johnston, N. R.; Jones, B. J.; Bloom, S. R.; Rutter, G. A.; Hoffmann-Roder, A.; Hodson, D. J.; Trauner, D. Optical Control of Insulin Secretion Using an Incretin Switch. *Angew. Chem. Int. Ed. Engl.* **2015,** *54*, 15565-15569.

29. Donthamsetti, P. C.; Winter, N.; Schonberger, M.; Levitz, J.; Stanley, C.; Javitch, J. A.; Isacoff, E. Y.; Trauner, D. Optical Control of Dopamine Receptors Using a Photoswitchable Tethered Inverse Agonist. *J. Am. Chem. Soc.* **2017,** *139*, 18522-18535.

30. Westphal, M. V.; Schafroth, M. A.; Sarott, R. C.; Imhof, M. A.; Bold, C. P.; Leippe, P.; Dhopeshwarkar, A.; Grandner, J. M.; Katritch, V.; Mackie, K.; Trauner, D.; Carreira, E. M.; Frank,

J. A. Synthesis of Photoswitchable Delta(9)-Tetrahydrocannabinol Derivatives Enables Optical Control of Cannabinoid Receptor 1 Signaling. *J. Am. Chem. Soc.* **2017,** *139*, 18206-18212.

31. Barber, D. M.; Liu, S. A.; Gottschling, K.; Sumser, M.; Hollmann, M.; Trauner, D. Optical Control of AMPA Receptors Using a Photoswitchable Quinoxaline-2,3-Dione Antagonist. *Chem. Sci.* **2017,** *8*, 611-615.

32. Stawski, P.; Sumser, M.; Trauner, D. A Photochromic Agonist of Ampa Receptors. *Angew. Chem. Int. Ed. Engl.* **2012,** *51*, 5748-5751.

33. Volgraf, M.; Gorostiza, P.; Numano, R.; Kramer, R. H.; Isacoff, E. Y.; Trauner, D. Allosteric Control of an Ionotropic Glutamate Receptor with an Optical Switch. *Nat. Chem. Biol.* **2006,** *2*, 47-52.

34. Volgraf, M.; Gorostiza, P.; Szobota, S.; Helix, M. R.; Isacoff, E. Y.; Trauner, D. Reversibly Caged Glutamate: A Photochromic Agonist of Ionotropic Glutamate Receptors. *J. Am. Chem. Soc.* **2007,** *129*, 260-261.

35. Cheng, B.; Shchepakin, D.; Kavanaugh, M. P.; Trauner, D. Photoswitchable Inhibitor of a Glutamate Transporter. *ACS. Chem. Neurosci.* **2017,** *8*, 1668-1672.

36. Quandt, G.; Hofner, G.; Pabel, J.; Dine, J.; Eder, M.; Wanner, K. T. First Photoswitchable Neurotransmitter Transporter Inhibitor: Light-Induced Control of Gamma-aminobutyric Acid Transporter 1 (GAT1) Activity in Mouse Brain. *J. Med. Chem.* **2014,** *57*, 6809-6821.

37. Podewin, T.; Broichhagen, J.; Frost, C.; Groneberg, D.; Ast, J.; Meyer-Berg, H.; Fine, N. H. F.; Friebe, A.; Zacharias, M.; Hodson, D. J.; Trauner, D.; Hoffmann-Roder, A. Optical Control

of a Receptor-Linked Guanylyl Cyclase Using a Photoswitchable Peptidic Hormone. *Chem. Sci.* **2017,** *8*, 4644-4653.

38. Frank, J. A.; Yushchenko, D. A.; Hodson, D. J.; Lipstein, N.; Nagpal, J.; Rutter, G. A.; Rhee, J. S.; Gottschalk, A.; Brose, N.; Schultz, C.; Trauner, D. Photoswitchable Diacylglycerols Enable Optical Control of Protein Kinase C. *Nat. Chem. Biol.* **2016,** *12*, 755-762.

39. Tsai, Y. H.; Essig, S.; James, J. R.; Lang, K.; Chin, J. W. Selective, Rapid and Optically Switchable Regulation of Protein Function in Live Mammalian Cells. *Nat. Chem.* **2015,** *7*, 554-561.

40. Zhang, Y.; Erdmann, F.; Fischer, G. Augmented Photoswitching Modulates Immune Signaling. *Nat. Chem. Biol.* **2009,** *5*, 724-726.

41. Blanco, B.; Palasis, K. A.; Adwal, A.; Callen, D. F.; Abell, A. D. Azobenzene-Containing Photoswitchable Proteasome Inhibitors with Selective Activity and Cellular Toxicity. *Bioorg. Med. Chem.* **2017,** *25*, 5050-5054.

42. Hansen, M. J.; Velema, W. A.; de Bruin, G.; Overkleeft, H. S.; Szymanski, W.; Feringa, B. L. Proteasome Inhibitors with Photocontrolled Activity. *Chembiochem* **2014,** *15*, 2053-2057.

43. Kim, Y.; Phillips, J. A.; Liu, H.; Kang, H.; Tan, W. Using Photons to Manipulate Enzyme Inhibition by an Azobenzene-Modified Nucleic Acid Probe. *Proc. Natl. Acad. Sci. U. S. A.* **2009,** *106*, 6489-6494.

44. Albert, L.; Xu, J.; Wan, R.; Srinivasan, V.; Dou, Y.; Vazquez, O. Controlled Inhibition of Methyltransferases Using Photoswitchable Peptidomimetics: Towards an Epigenetic Regulation of Leukemia. *Chem. Sci.* **2017,** *8*, 4612-4618.

45. Broichhagen, J.; Jurastow, I.; Iwan, K.; Kummer, W.; Trauner, D. Optical Control of Acetylcholinesterase with a Tacrine Switch. *Angew. Chem. Int. Ed. Engl.* **2014,** *53*, 7657-7660.

46. Reis, S. A.; Ghosh, B.; Hendricks, J. A.; Szantai-Kis, D. M.; Tork, L.; Ross, K. N.; Lamb, J.; Read-Button, W.; Zheng, B.; Wang, H.; Salthouse, C.; Haggarty, S. J.; Mazitschek, R. Light-Controlled Modulation of Gene Expression by Chemical Optoepigenetic Probes. *Nat. Chem. Biol.* **2016,** *12*, 317-323.

47. Herre, S.; Schadendorf, T.; Ivanov, I.; Herrberger, C.; Steinle, W.; Ruck-Braun, K.; Preissner, R.; Kuhn, H. Photoactivation of an Inhibitor of the 12/15-Lipoxygenase Pathway. *Chembiochem* **2006,** *7*, 1089-1095.

48. Velema, W. A.; van der Berg, J. P.; Hansen, M. J.; Szymanski, W.; Driessen, A. J.; Feringa, B. L. Optical Control of Antibacterial Activity. *Nat. Chem.* **2013,** *5*, 924-928.

49. Wegener, M.; Hansen, M. J.; Driessen, A. J. M.; Szymanski, W.; Feringa, B. L. Photocontrol of Antibacterial Activity: Shifting from UV to Red Light Activation. *J. Am. Chem. Soc.* **2017,** *139*, 17979-17986.

50. Zhang, F.; Timm, K. A.; Arndt, K. M.; Woolley, G. A. Photocontrol of Coiled-Coil Proteins in Living Cells. *Angew. Chem. Int. Ed. Engl.* **2010,** *49*, 3943-3946.

51. Hantschel, O.; Warsch, W.; Eckelhart, E.; Kaupe, I.; Grebien, F.; Wagner, K. U.; Superti-Furga, G.; Sexl, V. BCR-ABL Uncouples Canonical JAK2-STAT5 Signaling in Chronic Myeloid Leukemia. *Nat. Chem. Biol.* **2012,** *8*, 285-293.

52. Lai, A. C.; Toure, M.; Hellerschmied, D.; Salami, J.; Jaime-Figueroa, S.; Ko, E.; Hines, J.; Crews, C. M. Modular PROTAC Design for the Degradation of Oncogenic BCR-ABL. *Angew. Chem. Int. Ed. Engl.* **2016,** *55*, 807-810.

53. Demizu, Y.; Shibata, N.; Hattori, T.; Ohoka, N.; Motoi, H.; Misawa, T.; Shoda, T.; Naito, M.; Kurihara, M. Development of BCR-ABL Degradation Inducers Via the Conjugation of an Imatinib Derivative and a cIAP1 Ligand. *Bioorg. Med. Chem. Lett.* **2016,** *26*, 4865-4869.

54. Shibata, N.; Miyamoto, N.; Nagai, K.; Shimokawa, K.; Sameshima, T.; Ohoka, N.; Hattori, T.; Imaeda, Y.; Nara, H.; Cho, N.; Naito, M. Development of Protein Degradation Inducers of Oncogenic BCR-ABL Protein by Conjugation of ABL Kinase Inhibitors and IAP Ligands. *Cancer Sci.* **2017,** *108*, 1657-1666.

55. Zhao, Q.; Ren, C.; Liu, L.; Chen, J.; Shao, Y.; Sun, N.; Sun, R.; Kong, Y.; Ding, X.; Zhang, X.; Xu, Y.; Yang, B.; Yin, Q.; Yang, X.; Jiang, B. Discovery of Siais178 as an Effective BCR-ABL Degrader by Recruiting Von Hippel-Lindau (VHL) E3 Ubiquitin Ligase. *J. Med. Chem.* **2019,** *62*, 9281-9298.

56. Burslem, G. M.; Schultz, A. R.; Bondeson, D. P.; Eide, C. A.; Savage Stevens, S. L.; Druker, B. J.; Crews, C. M. Targeting BCR-ABL1 in Chronic Myeloid Leukemia by PROTAC-Mediated Targeted Protein Degradation. *Cancer Res.* **2019,** *79*, 4744-4753.

57. Tong, H.; Qi, D.; Guan, X.; Jiang, G.; Liao, Z.; Zhang, X.; Chen, P.; Li, N.; Wu, M. C-abl Tyrosine Kinase Regulates Neutrophil Crawling Behavior under Fluid Shear Stress Via Rac/PAK/LIMK/Cofilin Signaling Axis. *J. Cell. Biochem.* **2018,** *119*, 2806-2817.

58. Wang, X.; Wang, L.; Garcia, J. G. N.; Dudek, S. M.; Shekhawat, G. S.; Dravid, V. P. The Significant Role of c-abl Kinase in Barrier Altering Agonists-Mediated Cytoskeletal Biomechanics. *Sci Rep* **2018,** *8*, 1002.

59. Zandy, N. L.; Playford, M.; Pendergast, A. M. ABL Tyrosine Kinases Regulate Cell-Cell Adhesion through Rho GTPases. *Proc. Natl. Acad. Sci. U. S. A.* **2007,** *104*, 17686-17691.

60. Reuven, N.; Adler, J.; Porat, Z.; Polonio-Vallon, T.; Hofmann, T. G.; Shaul, Y. The Tyrosine Kinase c-abl Promotes Homeodomain-Interacting Protein Kinase 2 (HIPK2) Accumulation and Activation in Response to DNA Damage. *J. Biol. Chem.* **2015,** *290*, 16478-16488.

61. Daraiseh, S. I.; Kassardjian, A.; Alexander, K. E.; Rizkallah, R.; Hurt, M. M. C-abl Phosphorylation of Yin Yang 1's Conserved Tyrosine 254 in the Spacer Region Modulates Its Transcriptional Activity. *Biochim. Biophys. Acta. Mol. Cell. Res.* **2018,** *1865*, 1173-1186.

62. Qin, C.; Hu, Y.; Zhou, B.; Fernandez-Salas, E.; Yang, C. Y.; Liu, L.; McEachern, D.; Przybranowski, S.; Wang, M.; Stuckey, J.; Meagher, J.; Bai, L.; Chen, Z.; Lin, M.; Yang, J.; Ziazadeh, D. N.; Xu, F.; Hu, J.; Xiang, W.; Huang, L.; Li, S.; Wen, B.; Sun, D.; Wang, S. Discovery of Qca570 as an Exceptionally Potent and Efficacious Proteolysis Targeting Chimera (PROTAC) Degrader of the Bromodomain and Extra-Terminal (BET) Proteins Capable of Inducing Complete and Durable Tumor Regression. *J. Med. Chem.* **2018,** *61*, 6685-6704.

63. Qiu, X.; Sun, N.; Kong, Y.; Li, Y.; Yang, X.; Jiang, B. Chemoselective Synthesis of Lenalidomide-Based PROTAC Library Using Alkylation Reaction. *Org. Lett.* **2019,** *21*, 3838-3841.

64. Zhou, B.; Hu, J.; Xu, F.; Chen, Z.; Bai, L.; Fernandez-Salas, E.; Lin, M.; Liu, L.; Yang, C. Y.; Zhao, Y.; McEachern, D.; Przybranowski, S.; Wen, B.; Sun, D.; Wang, S. Discovery of a Small-Molecule Degrader of Bromodomain and Extra-Terminal (BET) Proteins with Picomolar Cellular Potencies and Capable of Achieving Tumor Regression. *J. Med. Chem.* **2018,** *61*, 462-481.

65. Kronke, J.; Fink, E. C.; Hollenbach, P. W.; MacBeth, K. J.; Hurst, S. N.; Udeshi, N. D.; Chamberlain, P. P.; Mani, D. R.; Man, H. W.; Gandhi, A. K.; Svinkina, T.; Schneider, R. K.; McConkey, M.; Jaras, M.; Griffiths, E.; Wetzler, M.; Bullinger, L.; Cathers, B. E.; Carr, S. A.; Chopra, R.; Ebert, B. L. Lenalidomide Induces Ubiquitination and Degradation of Ck1alpha in Del(5q) MDS. *Nature* **2015,** *523*, 183-188.

66. Teichmann, E.; Hecht, S. Shining a Light on Proteolysis Targeting Chimeras. *ACS. Cent. Sci.* **2019,** *5*, 1645-1647.

67. Martin, R.; Bryan, M.; Marleen, B.; Daniele, S.; Antonio, M.; Michele, P.; Dirk, T. PHOTACs Enable Optical Control of Protein Degradation. *ChemRxiv* **2019**, preprint, DOI: 10.26434/chemrxiv.8206688.v2.

68. Yuta, N.; Kristie, D.; Alexander, D. Optical Control of Small Molecule-Induced Protein Degradation. *ChemRxiv* **2019**, preprint, DOI: 10.26434/chemrxiv.8216714.v1.

69. Patrick, P.; Kusal T. G., S.; Craig M., C.; Erick, C. Reversible Spatiotemporal Control of Induced Protein Degradation by Bistable photoPROTACs. *ChemRxiv* **2019**, preprint, DOI: 10.26434/chemrxiv.8281469.v2.

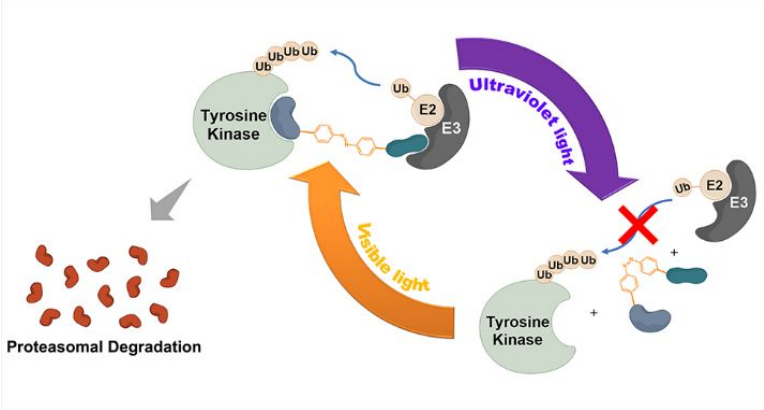

Table of Contents Graphic